Acta Biotheor (2016) 64:427–446
DOI 10.1007/s10441-016-9301-4

REGULAR ARTICLE

Discrete Mesh Approach in Morphogenesis Modelling: the Example of Gastrulation

J. Demongeot[1] · A. Lontos[2] · E. Promayon[2]

Received: 18 January 2016 / Accepted: 19 October 2016 / Published online: 16 November 2016
© Springer Science+Business Media Dordrecht 2016

Abstract Morphogenesis is a general concept in biology including all the processes which generate tissue shapes and cellular organizations in a living organism. Many hybrid formalizations (i.e., with both discrete and continuous parts) have been proposed for modelling morphogenesis in embryonic or adult animals, like gastrulation. We propose first to study the ventral furrow invagination as the initial step of gastrulation, early stage of embryogenesis. We focus on the study of the connection between the apical constriction of the ventral cells and the initiation of the invagination. For that, we have created a 3D biomechanical model of the embryo of the *Drosophila melanogaster* based on the finite element method. Each cell is modelled by an elastic hexahedron contour and is firmly attached to its neighbouring cells. A uniform initial distribution of elastic and contractile forces is applied to cells along the model. Numerical simulations show that invagination starts at ventral curved extremities of the embryo and then propagates to the ventral medial layer. Then, this observation already made in some experiments can be attributed uniquely to the specific shape of the embryo and we provide mechanical evidence to support it. Results of the simulations of the "pill-shaped" geometry of the *Drosophila*

Electronic supplementary material The online version of this article (doi:10.1007/s10441-016-9301-4) contains supplementary material, which is available to authorized users.

✉ J. Demongeot
Jacques.Demongeot@agim.eu

A. Lontos
Athanase.Lontos@imag.fr

E. Promayon
Emmanuel.Promayon@imag.fr

[1] AGIM, Faculty of Medicine of Grenoble, University J. Fourier, 38700 La Tronche, France

[2] TIMC-IMAG, Faculty of Medicine of Grenoble, University J. Fourier, 38700 La Tronche, France

melanogaster embryo are compared with those of a spherical geometry corresponding to the *Xenopus lævis* embryo. Eventually, we propose to study the influence of cell proliferation on the end of the process of invagination represented by the closure of the ventral furrow.

Keywords Discrete mesh modelling · Morphogenesis · Gastrulation · Ventral furrow

1 Introduction

Morphogenesis is a general concept in biology including all the processes which generate shapes and cellular organizations in a living organism referring to "birth of forms". Many models have been proposed for the morphogenesis in embryonic or adult animals (Allard et al. 2007; Bidhendi and Korhonen 2012; Bownes 1975; Brodland et al. 2010; Conte et al. 2007; Wang and Devarajan 2005; Davidson et al. 1999; Dawes-Hoang et al. 2005; Faure et al. 2007), like the gastrulation, taking into account all the factors responsible of the tissue genesis, for example those built by P. Tracqui and his coworkers (cf. obituary in Annex) and the general tendency since ten years is to offer a hybrid approach of the modelling having a discrete part (e.g., at cell proliferation, cytoskeleton organisation and genetic regulation levels) (Forest and Demongeot 2008; Forgacs and Newman 2005; Fouard et al. 2012) and a continuous part (e.g., at morphogen diffusion, enzymatic kinetics and cell migration levels) (Galle et al. 2005).

A very important stage of morphogenesis in animals is the gastrulation we will study in Sect. 2. The early embryo performs rapid cell divisions until the formation of the blastula, a geometrically simple closed elongated sphere or "pill-shaped" structure that consists of a single cell layer enclosing the hollow blastocœle (Forest and Demongeot 2008). Gastrulation includes mass movements of cells to form complex structures (e.g., tissues) from a simple initial shape (blastula). There are a number of inner cell structures that affect the cell movement and behaviour: (1) the cytoskeleton plays an important part in cellular motion and shape. It consists of three kinds of protein filaments: actin filaments, intermediate filaments and microtubules (Gumbiner 2005; Hardin and Keller 1988; Karr and Alberts 1986; Leptin 1999; Leptin and Grunewald 1990; Maniotis et al. 1997; Martin et al. 2008, 2010; Miyoshi and Takai 2008; Nesme et al. 2005; Oda and Tsukita 2000; Cui et al. 2005; Royou et al. 2004), (2) the Adherens Junctions (AJs) contain complexes of the transmembrane adhesion molecule E-cadherin and the adaptors α-catenin and ß-catenin (Galle et al. 2005; Maniotis et al. 1997). They are formed in the lateral surfaces of the cells and they offer strong links between neighbouring cells (Martin et al. 2008, 2010; Miyoshi and Takai 2008; Nesme et al. 2005), and (3) the myosin fibres are thin filaments found in the cytoskeleton of cells. They are flexible, versatile and relatively strong and they serve as tensile platforms for muscle contraction. One of the most important cell movements during gastrulation is the invagination of the ventral cells (also called primitive streak formation), which initiates the creation of the ventral furrow (Oda and Tsukita 2000; Cui et al. 2005;

Royou et al. 2004; Schejter and Wieschaus 1993). The process starts after the flattening of the cells on the ventral midline (Stephanou and Tracqui 2002). The myosin of the most ventrally located cells becomes concentrated at their apical sides (Davidson et al. 1999; Karr and Alberts 1986). This excess of myosin causes the constriction of their apical surface and a simultaneous apico-basal elongation. At this point, these cells move inwards and initiate the creation of the streak. A lot of research and bibliography have been dedicated to modelling the ventral furrow invagination. A very popular organism which has served as reference for these models is the *Drosophila melanogaster* (Conte et al. 2007; Faure et al. 2007; Stephanou and Tracqui 2002).

The main contribution of this work focuses on the study of the relationship between the apical constriction of the ventral cells and the invagination. We will analyze in Sect. 2.1 the effect of a factor that, to our knowledge, has not yet been extensively studied: the geometry of the embryo. For this purpose, we have created two 3D biomechanical models, one for the embryo of the *Drosophila melanogaster* ("pill-shaped") and one for the embryo of the *Xenopus lævis* (spherical), incorporating the previous mentioned factors: (1) cell elasticity due to the cytoskeleton, (2) strong bonds between cells due to AJs, and (3) contraction of the apical face due to myosin fibers. The in vivo phenomenon and the dynamic numerical simulations are compared to analyze the impact of the embryo's geometry on the invagination process. The comparison between the *Drosophila melanogaster* and the *Xenopus lævis* models will be done in Sect. 3. providing a better understanding of this impact.

2 Gastrulation

2.1 The Embryo Geometry

To ensure the specific shape of the *Drosophila melanogaster*'s embryo (Bownes 1975; Leptin 1999), we built a 3D biomechanical model composed by an elongated sphere (or "pill-shaped" mesh, symmetric along the antero-posterior and the dorso-ventral axis (cf. Fig. 1a–c), consisting of 2268 nodes forming 756 mono-layered hexahedra modelling the cells. The total length of the mesh is 460 μm and the diameter of its cross-section is 280 μm. The spherical mesh modeling the *Xenopus Laevis* embryo (Gumbiner 2005) consists of 904 nodes forming 450 mono-layered hexahedra (Fig. 1d). The diameter of its cross-section is 280 μm, same as the *Drosophila melanogaster*'s model. Each hexahedron is approximately 20 μm × 20 μm × 40 μm, resulting to an average volume of around 160 μm^3. Cells on the ventral midline area of the embryo (see outlined cells in Fig. 1a) are of particular interest in the invagination process. We distinguish two sub-areas of the ventral midline: the ventral medial layer (VML) and the ventral curved extremities (VCE), as described in Fig. 1c. The equivalence between the biological and in silico cells is presented in Table 1.

The behaviour of cells, defined as cellular objects in the simulation is controlled by three general principles: elasticity, contractility and incompressibility. Elasticity

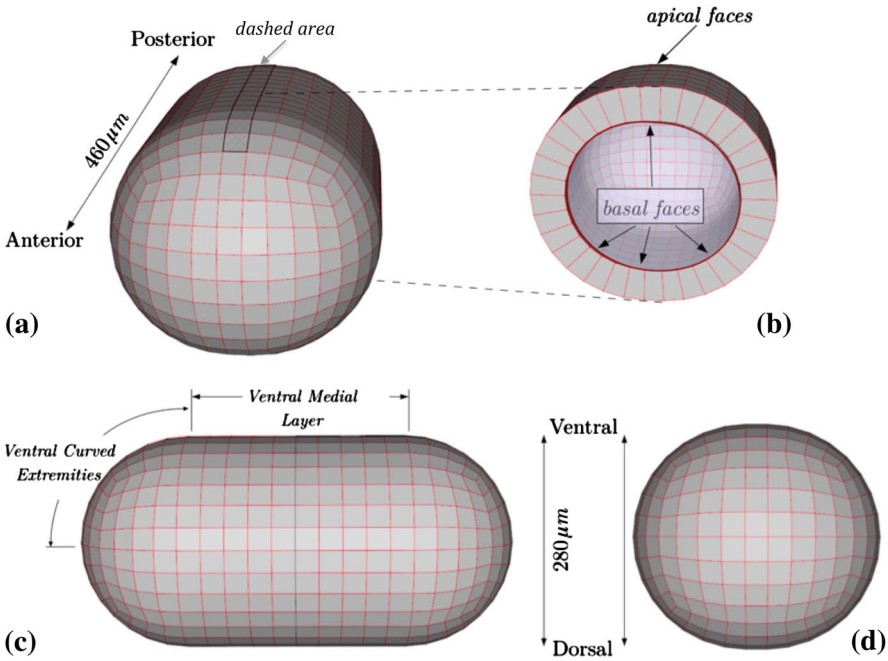

Fig. 1 The model of the *Drosophila melanogaster* embryo seen from an antero-ventral point of view (**a**). In **b** a cross-section of the model is presented showing the apical and basal faces of the cells. The *dashed* area highlights the ventral hexahedra, i.e., the hexahedra of the ventral area of the embryo submitted to an apical constriction. We distinguish two important areas in the model (**c**): the ventral medial layer (VML) and the ventral curved extremities (VCE). The spherical model of the *Xenopus Laevis* is presented in (**d**)

Table 1 Cell modelling

In vivo	In silico
Embryo of *Drosophila melanogaster*	"Pill-shaped" hexahedral mesh (756 hexahedra, 2268 nodes)
Embryo of *Xenopus laevis*	Spherical hexahedral mesh (450 hexahedra, 904 nodes)
Cell	Hexahedral cellular object composed of 8 nodes on the contour
Cytoskeleton	Elasticity of the hexahedra
Myosin fibres	Discrete springs offering contraction forces connecting the 4 active nodes of the apical surface of the hexahedron
Adherens junctions	Mesh connectivity (nodes are shared between neighbouring hexahedra)

and contractility are considered as forces applied on each particle corresponding to each of the 4 active nodes of the apical surface of the cell hexahedron, these nodes modelling the focal points on which are exerted these elasticity and contractility

forces produced by the neighbouring cells and denoted F_e and F_c respectively. Incompressibility is considered as a constraint that acts directly on the particles' positions.

2.2 Cell Elasticity

The general principle is that elasticity is based on a shape memory force applied to each particle depending on its connected particles (neighbours) and on the so called rest shape attractor, i.e., a reference cell state corresponding to the cell without deformation. The particles are modelling the focal points of application of the forces produced by neighbouring cells. Each particle is defined by a position, a mass, and a list of elastic properties. Let $P(t + 1)$ be the current position of a given particle at time $t + 1$ and $P_i(t)$, $i \in \{1, \ldots, n\}$ the positions of its n neighbouring particles at time t. The idea is to express the position $P(t + 1)$ as a function f of the positions $P_i(t)$ and of the position P^* of the particle in the rest shape attractor, with $v_i(t)$ denoting the vector $\mathrm{P}(t)P_i(t)$. f computes the position of a particle at time $(t + 1)$ based on the configuration of its neighbouring particles at time t and some scalars defined at rest shape, i.e., when the cell is not deformed. A single spring is used to generate an elastic force F_e that brings the particle towards its position in the rest shape attractor. The model is then similar to the spring model with preload described in Wang and Devarajan (2005): for a general spring connecting the considered particle to its ith neighbour particle, let denote by P_i^* the preload position of the considered node on the spring i, and by U_i the length of the ith spring when the mass-spring model is in its natural rest state. Consequently, the force F_{ei} exerted by the ith neighbouring particle is a function of the current position of the particle and the position of its preload attractor:

$$F_{ei}(t) = -\left(P_i^* + k_e(||v_i(t)|| - U_i)v_i(t)/||v_i(t)||\right),$$

where the Hooke's constant k_e is here defined as a simple scalar uniformly distributed along the particles.

2.3 Apical Constriction

The main characteristics of contractility taken into account in our model are: application particles, mechanical and electrical properties and, mainly, fibres generating contractility between particles. The principle used here is again a force created by an preload attractor due to the presence of a neighbouring particle located in the direction of the fibre. An internal contractile force F_c is then generated by the ith fibre and given by:

$$F_{ci}(t) = -\left(P_i^* + k_c(||v_i(t)|| - U_i)v_i(t)/||v_i(t)||\right),$$

where k_c is the contractility coefficient. It can vary during the simulation. A positive coefficient yields to an active contraction. When k_c is decreasing to zero, the contractile force is nullified and the cell returns to its original configuration, due to the elasticity property.

Each cell hexahedron can then be considered as an elastic element in a finite elements model (FEM) on which we apply the discrete Newton equation for getting the displacement of the considered particle using the balance of the forces $F_{ei}(t)$ and $F_{ci}(t)$ exerted on it (Wang and Devarajan 2005). All the cells are supposed to have the same properties and comparably equal initial volumes, regardless of their position in the structure, as well as the same elasticity constant: for the stress strain equation, we use a simple linear elasticity constitutive law with the same rather small Young modulus equal to 1000 Pa (Davidson et al. 1999). Concerning the Poisson ratio (of transverse contraction strain to longitudinal extension strain in the direction of stretching elastic force), we have chosen a conventionally used value in the bibliography of cell and soft tissue modelling close to 0.5 (Bidhendi and Korhonen 2012; Conte et al. 2007; Galle et al. 2005; Maniotis et al. 1997).

The domain of the flattened ventral zone where the invagination will occur is 70 %–80 % of the egg length (Sweeton et al. 1991). In order to simulate the apical constriction of the cells, contraction forces are generated between the nodes of the apical surface of each cell using discrete springs (Fig. 2). It should be noted that, to our knowledge, there is little experimental data regarding the value of the active forces that cells can generate at this stage of the morphogenesis. Brodland et al. (2010) aims to provide such data, but the direction of the forces in 3D is not specified. Consequently, the intensity of the contraction forces was optimized in order to conform to observed changes in shape (Oda and Tsukita 2000): it was chosen in order to induce a 30 % decrease of the apical surface of the cell located in the VML. The same value is applied to all the cells of the ventral area of the embryo

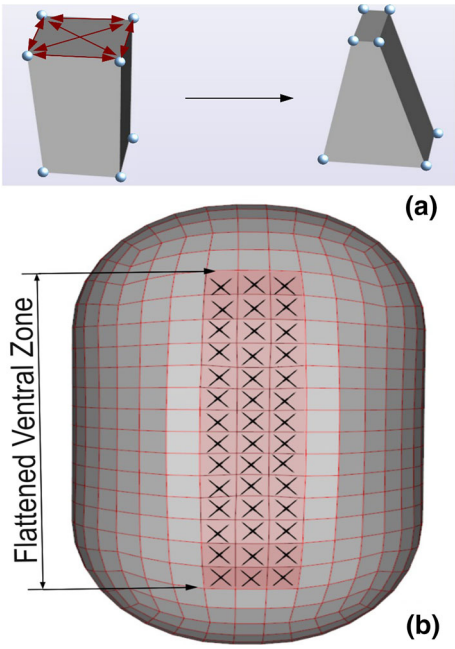

Fig. 2 **a** All the cells are modelled as easily deformable hexahedra. They are defined by 8 nodes located at the vertices of the hexahedra. For VML hexahedra, contraction forces are applied on the apical nodes (*red arrows*) to induce the apical constriction. The shape of the hexahedron changes, from an initial regular hexahedral shape (*left*) to a prismatic shape (*right*). **b** The most ventrally located cells of the model where contraction forces are added to their apical faces are highlighted (*pink colour* with *black cross*). The number of *rows* of hexahedra receiving this force can vary (in this case three *rows* are contractile representing a total area of $4 \times 14 \times 3 = 168\ \mu m^2$). (Color figure online)

(outlined row of cells in Fig. 1a) in order to ensure an equal initial distribution of forces along the antero-posterior axis of the structure.

2.4 Cell-to-Cell Bonds (AJs)

Adherens junctions (AJs) are binding neighbouring cells. They are formed in the lateral surfaces of the cells (Martin et al. 2008; Nesme et al. 2005; Sweeton et al. 1991). In our model, we have considered AJs to be located on the vertices of the cells (hexahedra) and to offer an unbreakable binding (Martin et al. 2010; Nesme et al. 2005). This is achieved by the mesh connectivity, which also allows a faster propagation of the forces during the simulation.

2.5 Incompressibility

In this section, we present the principle of the method implemented to control the volume of the cells. Consider the surface of an object in 3D represented by a mesh of triangles with n vertices. Let $P_1, \ldots, P_n$ be the positions of these vertices in a local referential defined by the sides of the triangle, and X the vector of size $3n$ composed by the positions of all these vertices: $X = (P_1, \ldots, P_n)$ is the vector describing the state of the polyhedron. Let $V(X(t))$ be the volume function of the mesh at time t with V_0 the initial volume. The technique implemented is as follows: suppose a deformation of the triangular mesh represented by the vector $X(t)$. The method implemented allows us to find a vector $X(t + \Delta t)$ from $X(t)$, whose volume is equal to V_0 (the initial volume). Consequently, what we need to do is to determine the displacement of each vertex, solving the following system:

$$X(t+\Delta t) = X(t) + \lambda \nabla V(X(t)), \text{ with } V(X(t+\Delta t)) = V_0,$$

where ∇V is the gradient of the volume V and λ is a scalar to be calculated (cf. Eq. 2). In the case of the Drosophila embryo, the system can be written as:

$$X_i(t+\Delta t) = X_i(t) + \lambda \nabla V(X_i(t)), \forall i \in \{1, \ldots, n\}, \text{ with } \sum_i V(X_i(t+\Delta t)) = V_0, \tag{1}$$

where $\nabla V(X_i(t))$ is the gradient of the ith component of the volume function. More precisely, if we denote $\overline{ij}(t)$ the vector between the vertices i and j at time t, then, if $i_1, \ldots, i_6$ are the 6 neighbours of i, then:

$$V(X_i(t)) = \langle X_i(t), A_i(t) \rangle, \text{ where } A_i(t) = \left[\sum_{k=1,6} \overline{ii_k}(t) \wedge \overline{ii_{k+1}}(t) \right] / 6$$

In a triangular mesh, it is possible to prove that: $\nabla V(X_i(t)) = A_i(t)$ and that the system (1) can be reduced thanks to the Newton equation to a 3rd degree equation in λ:

$$\lambda^3 \sum_i a_i + \lambda^2 \sum_i b_i + \lambda \sum_i c_i + \sum_i d_i - V_0 = 0. \quad (2)$$

The parameter λ is space and volume dependent, hence for example the V_0 variability influences the cell deformation. In further studies, this influence will be studied on the displacement $\Delta X_i(t) = \lambda \nabla V(X(t))$ of the vertex i of the mesh applied according to the λ value equal to the unique real root of Eq. (2) (Allard et al. 2007; Bidhendi and Korhonen 2012; Dawes-Hoang et al. 2005; Forgacs and Newman 2005; Miyoshi and Takai 2008). This equation is calculated after the Newton equation resulting from the balance of the forces F_{ei} and F_{ci} applied at each vertex i for controlling incompressibility to avoid a too important change of cell volume.

2.6 Cell Division

The term "mesh cutting" refers to modifying an existing mesh by moving nodes to a cutting entity and modifying the connectivity of the mesh so that the original mesh fits a new geometry. "Mesh segmentation" is the process of partitioning a mesh into more visually simple and meaningful components. Generally, users cut a meaningful component from its underlying mesh by specifying which parts of the mesh belong to the "foreground" (part to be cut out) and the rest to the background. Although it is quite easy for a human to specify foreground and background by saying something like "cut out the ears from the bunny model" to another human, the computer is still a long way from the sort of cognitive object understanding required to do this work unassisted. The major issues that a mesh cutting method needs to address are: (1) definition of the cut path, (2) element removal and re-meshing, (3) number of new elements created when re-meshing is performed and (4) representation of the cutting tool (Fig. 3).

In general, we can say that the mitotic procedure of an individual eucaryotic cell follows the following path:

- The mother cell arrives at a dividing state (either triggered by a mitogen, i.e., a chemical substance that encourages a cell to commence mitosis, or receiving an electrical signal (Blackiston et al. 2009) or by growing over a certain level).
- The mother cell is split into two daughter cells (for our simulation, we are going to assume that the two offsprings have the same size).
- The two new cells are temporary linked and share a common surface.
- The daughter cells inherit their mother's properties.
- The life of a cell ends with apoptosis (this aspect is of no interest for our model).

The main challenges of the hexahedral division that we had to address when dividing an hexahedral element corresponding to a cell and participating in the topology of a finite element mesh are (Fig. 4):

- To determine the direction of the division (cut)
- To make sure that the two new elements are well defined and placed in the topology

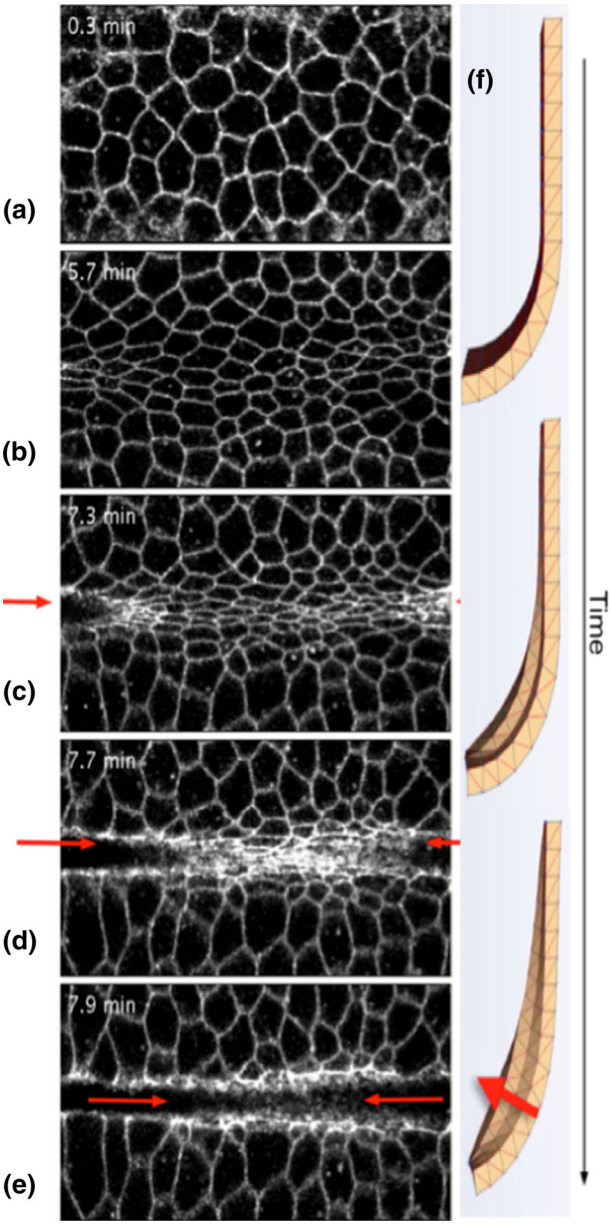

Fig. 3 Z-slices of cell membranes revealed with Spider-GFP showing the apical constriction of ventral cells followed by invagination (Martin et al. 2010). **a**, **b** Describe the first steps of the contraction along a longitudinal line, i.e., a generator of the embryo cylinder. With the *red arrows*. In **c**, we point out that the cells located in the extremities of the embryo are the first to invaginate and as they move towards the interior of the embryo, they disappear from the image. In **d**, the cells closer to the centre of the embryo move towards the interior as well, showing a propagation of the invagination from the extremities to the ventral medial layer. In **e**, the successive ventral profiles of the mesh are showing the progressive invagination going from the extremities to the centre of the embryo. (Color figure online)

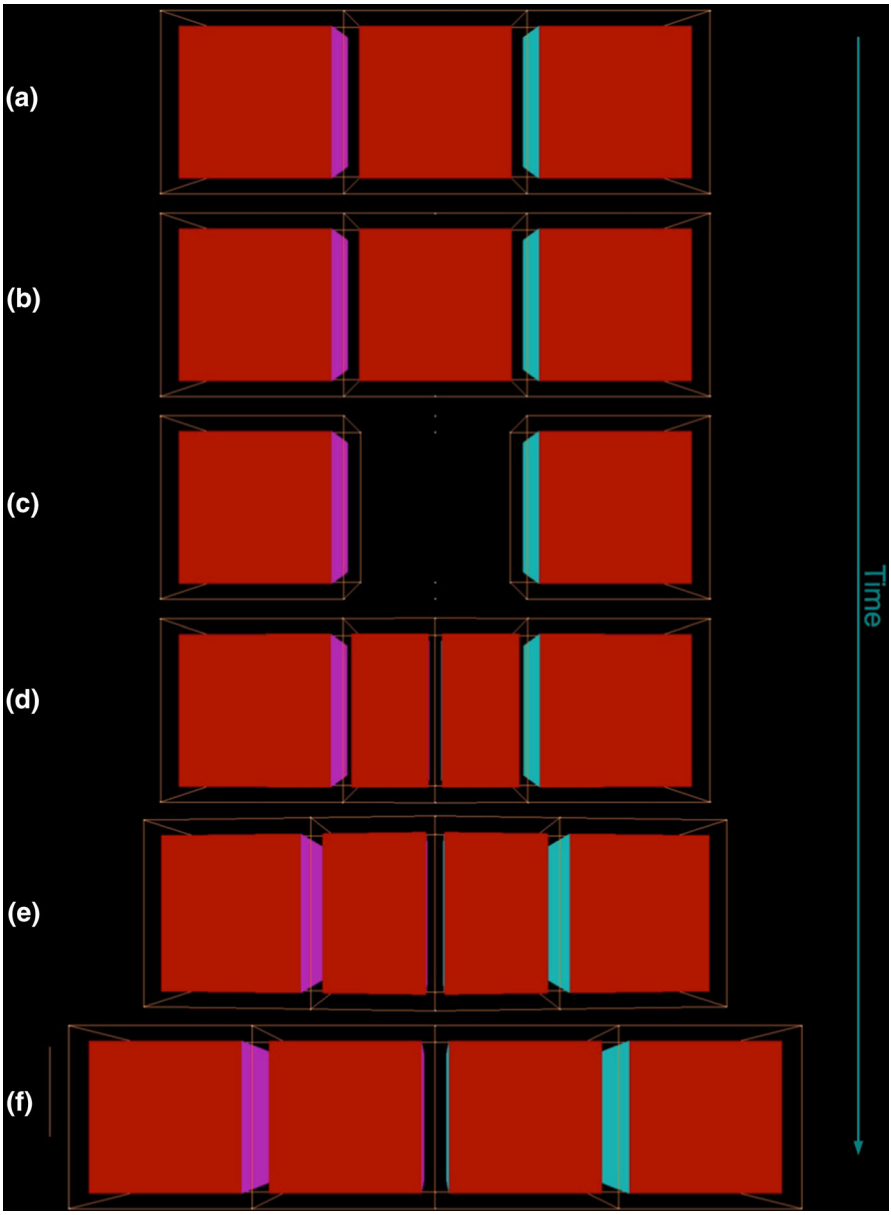

Fig. 4 Instances of an individual hexahedral division in a simple 3-hexahedron mesh. **a** The hexahedrons in their initial state. **b** The points that define the position of the cut in the mesh are positioned. **c** The mother middle hexahedron is removed. **d** The two daughter hexahedrons are placed in the mesh. **e** Daughter hexahedrons start to inflate for acquiring the original form of their mother. **f** Hexahedrons have acquired the same form as their mother, signalling the end of the process

- To make sure that they are close/linked to each other (share a facet or nodes of the mesh)
- To make sure that they will "try" to acquire the same size and shape that their mother originally had (rest shape).

The process of the division of a single hexahedron is shown in Fig. 4. We choose to divide the middle hexahedron in a very simple hexahedral mesh comprised of 3 hexahedrons. A linear constitutive law defines the elasticity of the mesh with a rather small Young modulus of $E = 1000\ Pa$ and a commonly used Poisson ratio close to $v = 0.5$. The values of the Young Modulus and the Poisson ratio are not essential in this particular example, they were chosen because we use the same values in the model of the *Drosophila melanogaster* embryo. The only existing forces are the elasticity forces of the finite element method; there are no external forces (gravity, superimposed forces from the user…). The direction of the division plane is vertical to the main axis of the mesh.

The comparison of the invagination process is given on Fig. 5, with (b) and without (c) cell division. Notice that the distance (green line) between the 2 nodes positioned higher than all others in the 2 meshes is smaller in (b) than in (c). Figure 6 shows an evidence of the existence of proliferation at the end of the invagination (Oda and Tsukita 2000).

2.7 Implementation

The simulation of the 3D biomechanical model of the embryo is performed by SOFA (an Open-Source Simulation Open Framework Architecture) (Allard et al. 2007; Dawes-Hoang et al. 2005) using CamiTK/MML2, an open-source framework, in order to compare and evaluate biomechanical simulations (Forgacs and Newman 2005). The hexahedral elements are implemented following the method described in Miyoshi and Takai (2008): the deformation of each element is decomposed into a rigid motion, a pure deformation, and a fast implicit dynamic integration without assembling a global stiffness matrix.

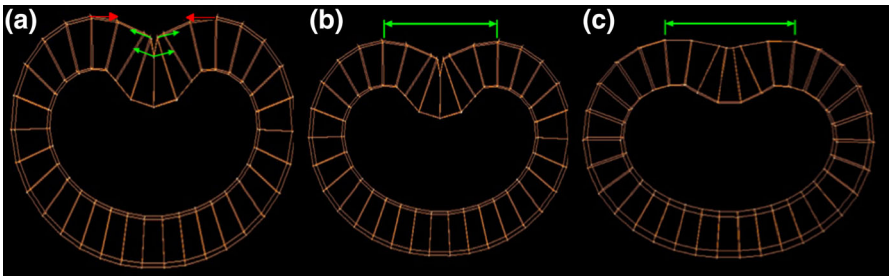

Fig. 5 **a** Configuration of forces for the embryo after the cell division. Daughter cells will try to expand their apical facet in order to acquire the initial parallelepiped shape of their mother. This would be done with elastic forces (*green arrows*) which, as a side-effect (notably due to the incompressibility), would cause the forces shown in red arrows to appear, driving ventral closure. **b**, **c** Show the result of the daughter cells expansion at the end of the process with cell division (**b**) and without cell division (**c**). (Color figure online)

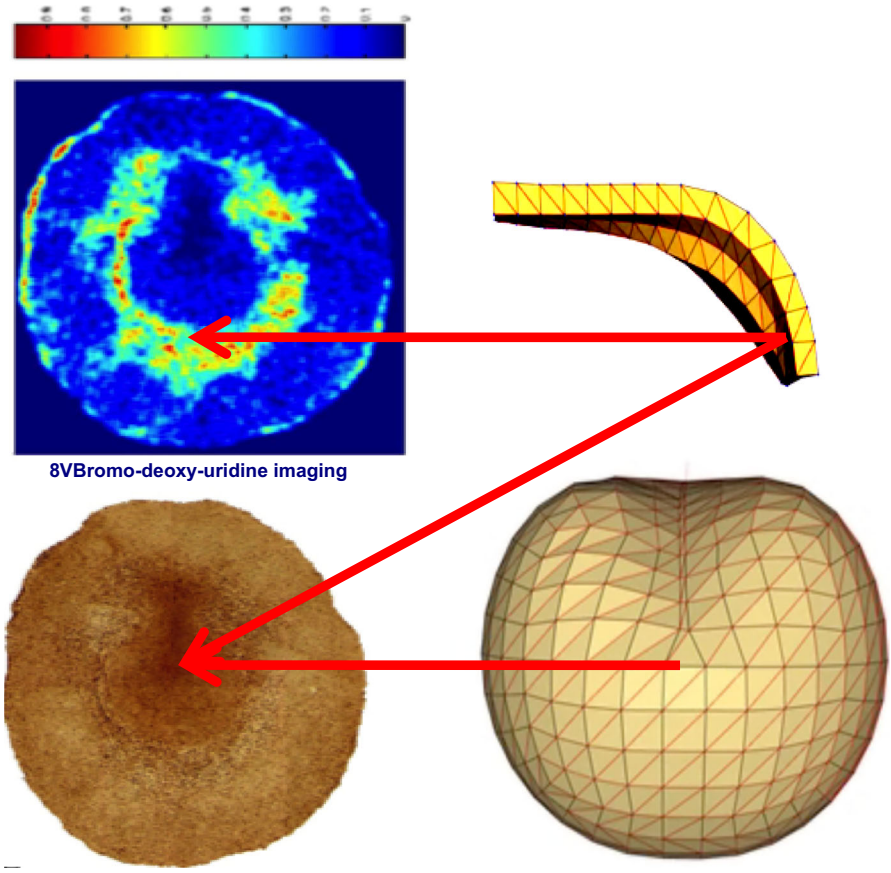

Fig. 6 Evidence of a proliferation activity shown by using Brdu incorporation imaging (Oda and Tsukita 2000) (*left*) on the extremities of the ventral furrow at the end of the invagination process (*right*)

The contractile forces are generated by an explicit 3D mass-spring network linking the nodes of the apical surface of each cell of the ventral area. Each spring uses a Kelvin–Voigt material, where a spring and a damper are acting in parallel. The linear system is solved dynamically using a conjugate gradient iterative algorithm. We define a state of equilibrium for our model when all nodal displacements are lower than 0.2 μm/s (at that point the simulation stops automatically). The resulting behaviour of combined soft elasticity and apical constriction is illustrated in Fig. 7 (see also Supplementary material). Thanks to MML, a set of values are monitored during the dynamic simulation that includes displacements and surfaces, in order to extract details concerning cell behaviour and motion.

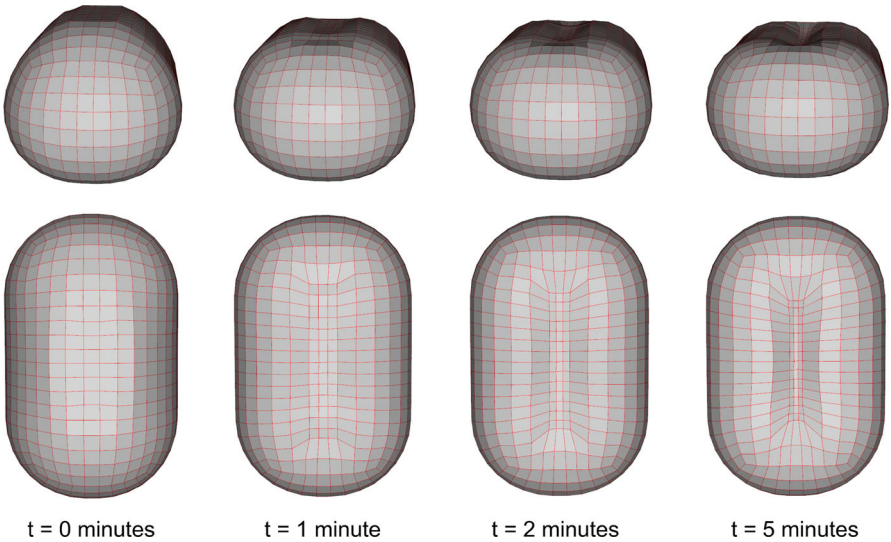

Fig. 7 Simulation of the ventral furrow invagination process on the "pill-shaped" embryo of *Drosophila melanogaster*. Instances of the geometry from an antero-ventral (*top*) and a ventral point of view (*bottom*). Notice the apical constriction of the ventral hexahedra which triggers the invagination

3 Comparison Between *Drosophila melanogaster* and *Xenopus lævis* Models

3.1 Invagination of the *Drosophila melanogaster* Embryo

The nodes of the apical face of the ventral hexahedra (Fig. 1b) are submitted to attractive forces of equal intensity (red arrows in Fig. 5). Figure 7 demonstrates four instances of the phenomenon from an antero-ventral and a ventral point of view. We notice that the invagination of the ventral hexahedra starts right after the initiation of their apical constriction. In addition, as they start to move inwards, they also pull the neighbouring hexahedra, thus increasing the invagination (Fig. 7). The observed total depth of the streak is 28.89 μm, consistent with in vivo studies of the phenomenon (Cui et al. 2005). Figure 8a demonstrates the comparison of the velocities of two hexahedra located at the VML and the VCE of the geometry respectively. The velocity of a hexahedron is measured by computing at each time-step of the simulation the displacement of its barycentre. Let v_m be the velocity of the hexahedron in the VML and v_c be the velocity of the hexahedron in the VCE. We notice that for the first 15 min the hexahedron in the VCE moves faster than the one in the VML ($v_c > v_m$). After 30 s, the difference between the velocities of the two hexahedra reaches its maximum value (approximately $v_c = 3.65v_m$). The model reaches a state of equilibrium after 15 min (Figs. 9, 10) when the stopping criterion of the simulation has been reached.

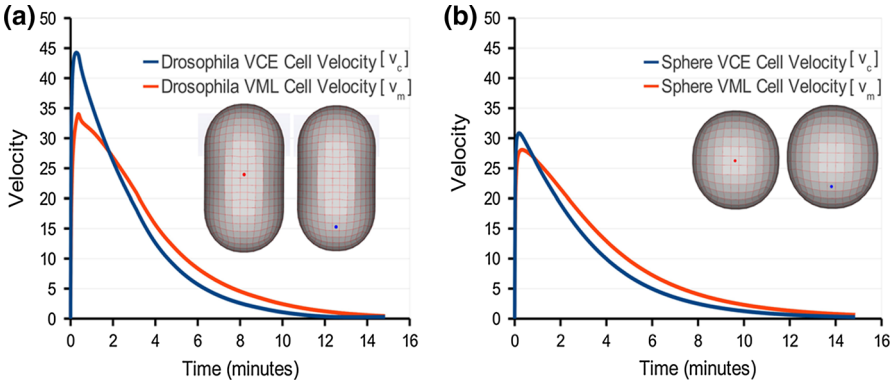

Fig. 8 The velocities of the barycentres of two cells located at the two areas of interest in the model of the *Drosophila melanogaster* (**a**) and in the model of the *Xenopus lævis* (**b**). Notice in **a** the faster movement of the barycentre in the VCE (*blue*) in the beginning and the equalization of the velocities after approximately t = 15 min. In **b**, the two barycentres have almost equal velocities throughout the simulation. (Color figure online)

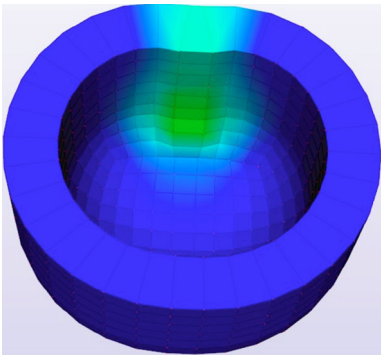

Fig. 9 Coloured cross-section of the *Drosophila melanogaster* model after t = 15 min. The *colour scale* corresponds to the intensity of the nodes displacements. (Color figure online)

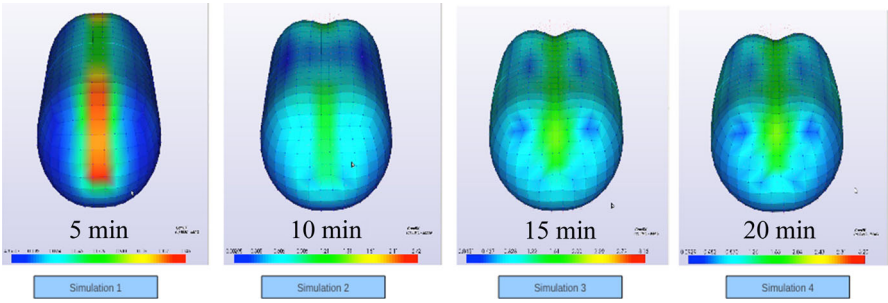

Fig. 10 Series of coloured top views of the *Drosophila melanogaster* model after t = 5, 10, 15, 20 min. The *colour scale* corresponds to the intensity of the nodes displacements. Cells that move the most intensely at the beginning are the cells located at the ends of the embryo. Then the invagination spreads throughout the blastula like in the experiments of the Fig. 3. (Color figure online)

3.2 Invagination of the *Xenopus laevis* Embryo

Figure 11 demonstrates four instances of the simulation from an antero-ventral and a ventral point of view. The observed total depth of the streak is 27.44 μm. Figure 8b demonstrates the comparison of the velocities of two cells, one located at the middle of the ventral midline (corresponding to the VML) and one located at the curved part (corresponding to the VCE). The velocities of the two barycentres are almost equal throughout the simulation, which means that the formation of the inner streak happens simultaneously along the spherical geometry. After 30 s, the difference of the velocities of the two hexahedra reaches its maximum value (approximately $v_c = 1.23\ v_m$).

3.3 External Constraints

The environment of the embryo is mainly composed by the vitelline layer (VL), the chorion and the yolk, that impact the cell movements. We model VL as a rigid external shell that surrounds the embryo and blocks outwards trajectories of the elements. In an other work (Conte et al. 2007), the yolk is modelled as a fluid which hinders the invagination, but there is not sufficient scientific data concerning its effect on the process. Thus, the yolk is not taken into account in our model.

4 Discussion

In Martin et al. (2010), the in vivo monitoring of the invagination in the *Drosophila melanogaster* shows that the area where the apical constriction starts and the area where the invagination starts differ (Fig. 3). In fact, the actin-myosin contractions occur first in the ventral medial layer (VML), while the invagination starts from the

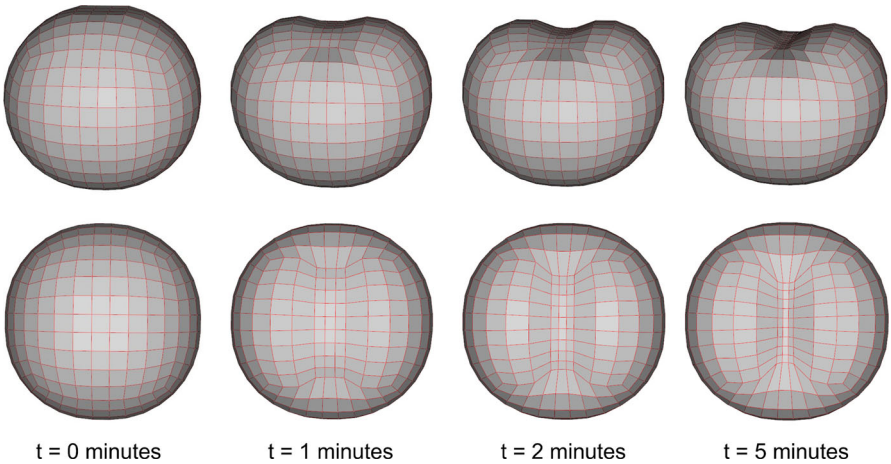

Fig. 11 Simulation of the invagination process on the spherical embryo *Xenopus laevis*. Instances of the geometry from an antero-ventral (*top*) and a ventral point of view (*bottom*)

ventral curved extremities (VCE) and then propagates to the VML. So the question remains: 'What makes the invagination start from the curved extremities?' In this work, we attempt to answer this question from a mechanical point of view only. First, we assume that the diffusion of myosin along the ventral area is so fast that all the cells start to constrict simultaneously. Nevertheless, we have shown that a centre node in the VCE displaces faster than a centre node in the VML (Fig. 8). The node displacements of the embryo after $t = 15$ s of simulation are represented by a colour scale in Figs. 9 and 10. The difference between the VCE and the VML is clearly visible: the displacement of the nodes in the VCE are in the (13–17) μm range while the displacements of the nodes in the VML are in the (7–10) μm range. We can conclude that despite the uniform initial distribution of forces along the ventral area of the model, the invagination is non-uniform following the process suggested in Martin et al. (2010).

In order to explain this observation, we need to take into consideration the geometry of the embryo. The asymmetry of the geometry in the VCE creates an imbalance of forces directed inwards generating an inward displacement of the node. The contracting forces applied on a node located at the VML do not generate any imbalance and therefore no displacement. The first nodes to move inwards are the nodes in the VCE. Their inward displacement later pulls the neighbouring cell nodes, causing the invagination to propagate towards the VML. This is confirmed by the simulation of the *Xenopus laevis* embryo where the formation of the inner streak is happening almost simultaneously along the spherical geometry (Fig. 8b).

Finally, the proliferation provides a way, experimentally proved, to complete the process of invagination. Figure 5 shows the existence of a force (represented by red arrows) exerted by the cells located on both sides of the gastrulation streak, reducing its diameter (Fig. 5b) if the proliferation takes place at bottom of the streak, with respect to the observed diameter in the absence of mitosis (Fig. 5c). Consideration should be given to a repeat of the proliferation to the upper border of the streak (as suggested by the experimental data in Fig. 6) so that these borders sufficiently closed permit the establishment of intercellular gap junctions corresponding to the closure of the gastric tube (Tepass and Hartenstein 1994). A non mechanical effect may also play a role, such as the genetic control of growth of filipodia leading to cell contacts at the top of the tube in formation (Mammoto and Ingber 2010), adhesive interactions between these filopodia causing the appearence of tethers ensuring the dorsal closure (Millard and Martin 2008).

The model is interesting in that it postulates a minima only the mechanical stress (mainly related to the elasticity and contractility of the concerned cells) to account for the early stages of formation of the streak during the gastrulation. Its shortcomings come from the insufficient consideration of the cell proliferation process and of the growth mechanisms of filipodia closing the roof of the gastric streak. Future work is undertaken from this perspective, taking into account the recent experimental works on the genetic control of the cytoskeleton of cells involved during gastrulation (Gjorevski and Nelson 2010; Navis and Bagnat 2015).

5 Conclusion

The ventral furrow invagination propagates from the ventral curved extremities to the ventral medial layer (cf. Fig. 11; Martin et al. 2010). The comparison of the simulations of the invagination process in the embryos of the *Drosophila melanogaster* and the *Xenopus lævis* shows that the geometry of the embryo plays an important role. From a biomechanical point of view, we suggest that the "pill-shaped" geometry of the embryo of the *Drosophila melanogaster* as well as the mechanical stress exerted on this shape mainly by elastic and contractile cellular forces are responsible for the sequence experimentally observed of the invagination propagation.

Acknowledgments We thank VHP NoE (EC) and MEC grant from CONICYT (Chile) for financially aiding our research.

Annex: P. Tracqui's Obituary

P. Tracqui died in 2015 leaving the French community of Theoretical Biology very sad and orphan. Philip left a very important work covering many fields of modelling in biomedicine: osteogenesis, wound healing, cell movement, tissue morphogenesis, carcinogenesis, with many seminal articles. He published a total of 40 articles in international journals of high level cited as reference works [cf. for example (Tracqui et al. 1995; Tracqui and Mendjeli 1999; Tracqui 2006; Tracqui et al. 2005; Tranqui and Tracqui 2000; Vailhe et al. 1997; Woodward et al. 1996)], usually with prominent co-authors. His students, his friends, his colleagues in Paris and Grenoble, in the Dynacell team of the laboratory TIMC-IMAG he founded and he directed with great science and humanity, will infinitely regret him.

P. Tracqui in 2014

Eventually, the authors of the present paper, friends of Philippe, recall some words in French pronounced by Philippe's spouse Valérie at the funerals (with her permission):

Philippe, toi le CHERCHEUR qui a marché ta Vie sur de multiples chemins…

Tu es né à Modane en 1956, dans une famille venant de Bessans, au fond de la vallée de la Maurienne. Tu étais un Être aux multiples talents, doué d'une grande intelligence et d'une formidable mémoire, ton exigence était à la hauteur de ton « commandeur » intérieur.

Tes passions?

La photographie Très tôt, ton regard fin a eu envie de photographier les instants d'éternité, les couleurs, les paysages de nature, les ambiances, les visages et tu as ainsi capté des milliers d'images, pour qu'elles restent pour toujours gravées en toi. Et pourquoi choisir un appareil photo plutôt qu'un autre? Tu préférais les posséder tous, avec tous les objectifs qui allaient avec, histoire de garder tous les possibles…

La musique et les sons Tu avais une oreille hors du commun, capable de repérer la moindre dissonance et de faire des réglages infinis pour améliorer la qualité des sons. Et ce fut une vraie joie quand à la fin de ta vie, tu révélais ta voix, si chaleureuse et juste, aussi bien sur tes poèmes que pour faire des sons. Tu jouais du piano, de la guitare, un peu de basse, des percussions… et possédais un labo d'enregistrement digne d'un professionnel…

Le sport Pour maintenir ton corps actif et surtout ne pas vieillir, ta hantise ! Marcher vite, pédaler dur, courir longtemps… l'exigence est toujours là!

La recherche scientifique Chercheur, tu étais très apprécié de tes collaborateurs. Capable à la fois d'une vision large et d'une détermination à aller dans les détails, tu allais chercher derrière les phénomènes de surface leurs processus et leurs causes. Tous les sujets t'intéressaient et tu menais tout de front: l'ordre et le chaos, la cicatrisation et… les mécanismes du cancer. Très reconnu dans le monde scientifique, tu as reçu en 1998 un prix de l'Académie des Sciences.

En tout, tu préférais la diversité, peut être par peur de manquer quelque chose?

Homme aux multiples talents, grand poète, musicien, peintre, photographe et sportif, tu marchais sur toutes les routes à la fois, au risque de t'épuiser et de ne pas te trouver. Ce cancer qui a touché tes os, c'est-à-dire la structure de qui tu croyais être (et que tu as tant étudiée au début de ta carrière de chercheur), fut terrible physiquement, mais ce fut une métamorphose pour ton éveil de conscience: tu as découvert le pouvoir de tes pensées sur le corps et le monde des illusions. Tu te réjouissais de témoigner de ton expérience au monde scientifique, mais, tu n'en as pas eu le temps, car la guérison ne touche pas forcément le corps physique, quand elle se dévoile à l'Esprit…

References

Allard J, Cotin S, Faure F, Bensoussan P, Poyer F, Duriez C, Delingette H, Grisoni L (2007) Sofa—an open source framework for medical simulation. In: Westwood JD, Haluck RS, Hoffman HM, Mogel

GT, Phillips R, Robb RA, Vosburgh KG (eds) 15th medicine meets virtual reality. IOP Press, Bristol, pp 13–18

Bidhendi A, Korhonen R (2012) A finite element study of micropipette aspiration of single cells: effect of compressibility. Comput Math Methods Med. doi:10.1155/2012/192618

Blackiston DJ, McLaughlin KA, Levin M (2009) Bioelectric controls of cell proliferation. Cell Cycle 8:3519–3528

Bownes M (1975) A photographic study of development in the living embryo of *Drosophila melanogaster*. J Embryol Exp Morphol 33:789–801

Brodland G, Conte V, Cranston P, Veldhuis J, Narasimhan S, Hutson M, Jacinto A, Ulrich F, Baum B, Miodownik M (2010) Video force microscopy reveals the mechanics of ventral furrow invagination in drosophila. Proc Natl Acad Sci 107:22111–22116. doi:10.1073/pnas.1006591107

Conte V, Munoz J, Miodownik M (2007) A 3D finite element model of ventral furrow invagination in the *Drosophila melanogaster* embryo. J Mech Behav Biomed Mater 1:188–198

Cui C, Yang X, Chuai M, Glazier JA, Weijer CJ (2005) Analysis of tissue flow patterns during primitive streak formation in the chick embryo. Dev Biol 284:37–47

Davidson L, Oster G, Keller R, Koehl M (1999) Measurements of mechanical properties of the blastula wall reveal which hypothesized mechanisms of primary invagination are physically plausible in the sea urchin *Strongylocentrotus purpuratus*. Dev Biol 209:221–238. doi:10.1006/dbio.1999.9249

Dawes-Hoang R, Parmar K, Christiansen A, Phelps C, Brand A, Wieschaus E (2005) Folded gastrulation, cell shape change and the control of myosin localization. Development 132:4165–4178. doi:10.1242/dev.01938

Faure F, Allard J, Cotin S, Neumann P, Bensoussan P, Duriez C, Delingette H, Grisoni L (2007) Sofa: a modular yet efficient simulation framework. In: Surgetica. (ed) Computer-aided medical interventions: tools and applications. Sauramps Médical, Paris

Forest L, Demongeot J (2008) A general formalism for tissue morphogenesis based on cellular dynamics and control system interactions. Acta Biotheor 56:51–74. doi:10.1007/s10441-008-9030-4

Forgacs G, Newman S (2005) Biological physics of the developing embryo. Cambridge University Press, Cambridge. doi:10.2277/0521783372

Fouard C, Deram A, Keraval Y, Promayon E (2012) CamiTK: a modular framework integrating visualization, image processing and biomechanical modelling. In: Payan Y (ed) Studies in mechanobiology, tissue engineering and biomaterials, vol 11. Springer, Berlin, pp 323–354

Galle J, Loeffler M, Drasdo D (2005) Modeling the effect of deregulated proliferation and apoptosis on the growth dynamics of epithelial cell populations in vitro. Biophys J 88:62–75

Gjorevski N, Nelson CM (2010) The mechanics of development: models and methods for tissue morphogenesis. Birth Defects Res C Embryo Today 90:193–202

Gumbiner B (2005) Regulation of cadherin-mediated adhesion in morphogenesis. Nat Rev Mol Cell Biol 6:622–634. doi:10.1038/nrm1699

Hardin J, Keller R (1988) The behaviour and function of bottle cells during gastrulation of *Xenopus laevis*. Development 103:211–230

Karr T, Alberts B (1986) Organization of the cytoskeleton in early drosophila embryos. J Cell Biol 102:1494–1509. doi:10.1083/jcb.102.4.1494

Leptin M (1999) Gastrulation in drosophila: the logic and the cellular mechanisms. EMBO J 18:3187–3192. doi:10.1093/emboj/18.12.3187

Leptin M, Grunewald B (1990) Cell shape changes during gastrulation in drosophila. Development 110:73–84

Mammoto T, Ingber DE (2010) Mechanical control of tissue and organ development. Development 137:1407–1420

Maniotis A, Chen C, Ingber D (1997) Demonstration of mechanical connections between integrins, cytoskeletal filaments, and nucleoplasm that stabilize nuclear structure. Proc Natl Acad Sci 94:849–854

Martin A, Kaschube M, Wieschaus E (2008) Pulsed contractions of an actin-myosin network drive apical constriction. Nature 457:495–499. doi:10.1038/nature07522

Martin A, Gelbart M, Fernandez-Gonzalez R, Kaschube M, Wieschaus E (2010) Integration of contractile forces during tissue invagination. J Cell Biol 188:735–749. doi:10.1083/jcb.200910099

Millard TH, Martin P (2008) Dynamic analysis of filopodial interactions during the zippering phase of Drosophila dorsal closure. Development 135:621–626

Miyoshi J, Takai Y (2008) Structural and functional associations of apical junctions with cytoskeleton. Biochim Biophys Acta (BBA) Biomembranes 1778:670–691. doi:10.1016/j.bbamem.2007.12.014

Navis A, Bagnat M (2015) Developing pressures: fluid forces driving morphogenesis. Curr Opin Genet Dev 32:24–30

Nesme M, Marchal M, Promayon E, Chabanas M, Payan Y, Faure F (2005) Physically realistic interactive simulation for biological soft tissues. Recent Res Dev Biomech 2:1–22

Oda H, Tsukita S (2000) Real-time imaging of cell-cell adherens junctions reveals that drosophila mesoderm invagination begins with two phases of apical constriction of cells. J Cell Sci 114:493–501

Royou A, Field C, Sisson J, Sullivan W, Karess R (2004) Reassessing the role and dynamics of non-muscle myosin ii during furrow formation in early drosophila embryos. Mol Biol Cell 15:838–850. doi:10.1091/mbc.E03-06-0440

Schejter E, Wieschaus E (1993) Functional elements of the cytoskeleton in the early drosophila embryo. Annu Rev Cell Biol 9:67–99. doi:10.1146/annurev.cb.09.110193.000435

Stephanou A, Tracqui P (2002) Cytomechanics of cell deformations and migration: from models to experiments. C R Biol 325:295–308

Sweeton D, Parks S, Costa M, Wieschaus E (1991) Gastrulation in drosophila: the formation of the ventral furrow and posterior midgut invaginations. Development 112:775–789

Tepass U, Hartenstein V (1994) The development of cellular junctions in the drosophila embryo. Dev Biol 161:563–596

Tracqui P (2006) Mechanical instabilities as a central issue for in silico analysis of cell dynamics. Proc IEEE Soc 94:710–724

Tracqui P, Mendjeli M (1999) Modelling 3-dimensional growth of brain tumours from time series of scans. Math Models Methods Appl Sci 9:581–598

Tracqui P, Cruywagen GC, Woodward DE, Bartoo GT, Murray JD, Alvord EC Jr (1995) A mathematical model of glioma growth: the effect of chemotherapy on spatio-temporal growth. Cell Prolif 28:17–31

Tracqui P, Namy P, Ohayon J (2005) Cellular networks morphogenesis induced by mechanically stressed microenvironments. J Biol Phys Chem 5:57–69

Tranqui L, Tracqui P (2000) Mechanical signaling and angiogenesis: the integration of cell—extracellular matrix couplings. C R Acad Sci Sér III 322:1–17

Vailhe B, Ronot X, Tracqui P, Usson Y, Tranqui L (1997) In vitro angiogenesis is modulated by the mechanical properties of fibrin gels and is related to αvβ3 integrin localization. Vitro Cell Dev Biol Animal 33:763–773

Wang X, Devarajan V (2005) 1D and 2D structured mass-spring models with preload. Visual Comput 21:429–448. doi:10.1007/s00371-005-0303-5

Woodward DE, Cook J, Tracqui P, Cruywagen GC, Murray JD, Alvord EC Jr (1996) A mathematical model of glioma growth: the effect of extent of surgical resection. Cell Prolif 29:269–288. doi:10.1111/j.1365-2184.1996.tb01580.x